Selective oxidation of alcohols with oxygen on Ru–Co-hydroxyapatite: A mechanistic study

Z. Opre, J.-D. Grunwaldt, T. Mallat, A. Baiker *

Department of Chemistry and Applied Biosciences, Swiss Federal Institute of Technology, ETH Hönggerberg, CH-8093 Zürich, Switzerland

Abstract

The chemical nature of the active ruthenium species and the mechanism of the oxidation of alcohols on Co-promoted Ru-hydroxyapatite have been investigated by in situ and ex situ EXAFS and kinetic analysis (reaction order of alcohol and oxygen, competing hydrogenation of primary and secondary alcohols, dehydrogenation in the absence of oxygen, kinetic isotope effect, Hammett study). It is concluded that the probable active sites are dihydroxo-ruthenium species (instead of $RuCl^{2+}$ as suggested earlier) and only about half of them are accessible to the reactant benzyl alcohol. The oxidative dehydrogenation reaction obeys the Mars–van Krevelen mechanism and the reduced hydrido-ruthenium species is inactive in alcohol dehydrogenation without reoxidation by molecular oxygen. In the catalytic cycle, the rate limiting step is either the β-hydride elimination step from the alcoholate or reoxidation of the ruthenium-hydride species, depending on the reaction conditions.
© 2005 Elsevier B.V. All rights reserved.

Keywords: Promoted Ru-hydroxyapatite; Aerobic oxidation; Benzylic alcohols; Mechanism; In situ EXAFS

1. Introduction

Selective oxidation of alcohols to aldehydes and ketones is an important transformation in synthetic chemistry. From environmental and technical points of view, an attractive solution is the application of a recyclable solid catalyst and molecular oxygen as the sole oxidant [1–4]. Partial oxidation of alcohols with transition metals bound to hydroxyapatite ($Ca_{10}(PO_4)_6(OH)_2$, HAp) fulfils these requirements of "green" chemistry [5].

Hydroxyapatite-based materials attracted increasing interest as solid catalysts. The acid–base properties of hydroxyapatite were used in various reactions including dehydration and dehydrogenation of alcohols [6,7], oxidation of alkanes [8,9], Knoevenagel condensation [10], Friedel-Crafts alkylation [11], and Michael addition [12]. Hydroxyapatite is used also as catalyst support for transition metal catalysts in various types of oxidation and carbon–carbon bond forming reactions [5]. Two classes of these catalysts can be distin-

guished: supported metals containing small Pd, Ru, or Au particles [13–15] and "ion-exchanged" materials, where transition metal ions are incorporated in the phosphate framework via soaking hydroxyapatite in a metal ion solution [16–20]. Note that formation of the metal-exchanged hydroxyapatite is a far more complex process than a simple ion-exchange [21,22].

A characteristic feature of ion-exchanged Ru-hydroxyapatites (RuHAp) is their high stability during catalytic oxidation reactions. The isolated Ru species are strongly coordinated to the apatite framework [16], in contrast to supported Pd^{2+} species that are reduced to Pd^0 by the reactant during alcohol oxidation [13]. We have shown recently [19] that Co- and Pb-promoted Ru-hydroxyapatite catalysts, prepared by fine tuning the location and surroundings of the active Ru site, are remarkably more active than RuHAp [16] and oxidize various alcohols to carbonyl compounds without by-product formation.

The structure of the active Ru species is still under discussion. Kaneda and co-workers suggested that the active sites are probably monomeric $RuCl^{2+}$ cations surrounded by O atoms of the phosphate matrix [16]. They adopted the

* Corresponding author. Tel.: +41 1 632 3153; fax: +41 1 632 1163.
E-mail address: baiker@chem.ethz.ch (A. Baiker).
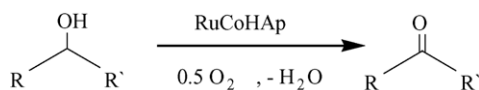
Scheme 1. Oxidation of alcohols to aldehydes with molecular oxygen on a Co-promoted ruthenium-hydroxyapatite (RuCoHAp) catalyst.

hydridometal pathway [23–26] and suggested that the alcohol oxidation was initiated by formation of a Ru–alcoholate species and followed by β-hydride elimination to produce the carbonyl compound in the rate-determining step. The co-product Ru-hydride species was reoxidized by molecular oxygen in the last step of the catalytic cycle. Note that according to this model the formation of the Ru–alcoholate species (Eq. (1)) would be accompanied by the equimolar formation of HCl and hydroxyapatite is unstable in acidic medium [27,28].

$$RuCl^{2+} + R–CH_2–OH \rightleftharpoons Ru^{2+}–O–CH_2–R + HCl \qquad (1)$$
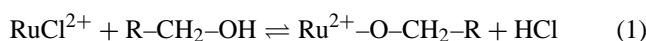
Besides, recent studies by X-ray photoelectron spectroscopy (XPS) and inductively coupled plasma optical emission spectroscopy (ICP-OES) question the presence of significant amount of Cl in RuHAp [18,19].

We assumed [19] that the active sites of promoted and unpromoted RuHAp catalysts were isolated Ru^{3+} ions, possibly Ru^{3+} hydroxo species, to compensate for the charge imbalance, when Ca^{2+} ions are substituted in hydroxyapatite [22]. The catalytic activity in alcohol oxidation was partially lost by drying the catalyst at temperatures above $80\,^\circ C$, presumably, due to irreversible dehydration of the active species [19], which observation supports the participation of ruthenium hydroxo species.

Here, we report a reinvestigation of the chemical nature of the active Ru species and the probable mechanism of alcohol oxidation using a Co-promoted Ru-hydroxyapatite (RuCoHAp) catalyst described in our previous paper (Scheme 1) [19]. Kinetic studies under typical reaction conditions were completed with analysis by extended X-ray absorption near-edge structure spectroscopy (EXAFS), including in situ studies in a continuous-flow reactor during oxidation of benzyl alcohol. Note that in situ EXAFS has been widely applied to study gas–solid type reactions [29–33] and more recently also liquid–solid reactions [34–37].

2. Experimental

2.1. Materials

Benzyl alcohol (>99%, Fluka), 4-nitrobenzyl alcohol (99%, Acros), 4-chlorobenzyl alcohol (99%, Acros), 4-methoxybenzyl alcohol (>98%, Acros), 4-methylbenzyl alcohol (99%, ABCR), benzyl alcohol-d7 ($C_6D_5CD_2OH$, 98 at.% D, Aldrich), 1-octanol (Acros), 2-octanol (Acros), toluene (Baker), RuO_x/Al_2O_3 (Engelhard), RuO_2 (ABCR),

RuCl₃ (ABCR), and mesitylene (99%, Acros) were used as received. The molecular sieve (Z4-01, Zeochem, AG) was activated at $200\,^\circ C$ in vacuum for 5 h before use.

The RuCoHAp catalyst was prepared according to our previous paper [19] (its abbreviation there was RuCoHAp-24 h). HAp, calcined at $500\,^\circ C$, was shaken with an aqueous solution of $CoCl_2$ for 20 min. The solid (CoHAp) was filtered off and washed with deionized water. Ruthenium was introduced by shaking the wet material with aqueous $RuCl_3$ solution at room temperature for 24 h. The RuCoHAp catalyst was filtered off, washed with deionized water, and dried for 8 h at $80\,^\circ C$ in vacuum. The relatively low drying temperature is necessary to minimize dehydration and restructuring. Details on the preparation of unpromoted RuHAp and the influence of contact time between HAp and the $RuCl_3$ solution on the structural and catalytic properties can be found elsewhere [19].

2.2. General oxidation procedure

The slurry containing 60 mg RuCoHAp (Ru: 0.021 mmol) in 10 ml toluene was stirred for 5 min under oxygen in a 50 ml glass reactor in the presence of oxygen at room temperature and atmospheric pressure. Then, the reactor was placed in a preheated oil bath and after 5 min the alcohol reactant was added to start the reaction. The selectivity and conversion were determined by GC analysis (Thermo Quest Trace 2000, equipped with an HP-FFAP capillary column and FID detector) using mesitylene as internal standard, and the products were identified by authentic samples. The initial reaction rates were calculated from the conversions up to 5%. In some cases, some molecular sieve was also added to the reaction mixture to minimize the effect of co-product water at conversions higher than ca. 5% (see later).

The reactor was operated under two typical conditions. Under condition I, high oxygen concentration (atmospheric pressure, $p(O_2) = 0.81$ bar) and efficient stirring ($1500\,min^{-1}$), where applied. No influence of the stirring frequency on the reaction rate could be detected in this regime. Condition II is characterized by low surface oxygen concentration achieved by applying air instead of oxygen (atmospheric pressure, $p(O_2) = 0.16$ bar) and low stirring frequency ($100\,min^{-1}$). The partial pressure of the solvent at the reaction temperature has been taken into consideration in the calculation of the oxygen partial pressure.

2.3. X-ray absorption (XAS) measurements

XAS spectra were recorded in the transmission geometry at HASYLAB, DESY (Hamburg, Germany) at beamline X1 with the use of a Si(3 1 1) double crystal monochromator. The storage ring was operated at 4.45 GeV with injection currents of 140 mA. Higher harmonics were effectively removed by detuning the crystals to 60% of the maximum intensity. Three ionization chambers, filled with Ar, were used for recording the intensity of the incident and the transmitted X-rays. The

samples were located between the first and second ionization chamber, a reference sample (RuCl₃ pellet) was placed between the second and the third ionization chamber. The in situ experiments were conducted in a continuous-flow reactor cell, described previously [36,37]. The RuCoHAp catalyst (52 mg) was loaded into the reactor cell. The reaction mixture (0.24 g benzyl alcohol in 100 ml toluene) and pure toluene were stored in two separate glass bubble tanks, where the liquids could be saturated with Ar or air. Liquids were provided from the tanks to the reactor by a peristaltic pump (ISMATEC Reglo 100) at a flow rate of $1.19\,\text{ml min}^{-1}$. During alcohol oxidation at fixed reaction parameters (stationary conditions), the flow rate of the feed was decreased to one-half. More details of the experimental setup can be found in previous reports [36,37].

When working with sample pellets and in situ under stationary conditions, EXAFS spectra were taken in the step-scanning mode around the Ru K-edge (22.117 keV) between 21.9 and 22.8 keV using a RuCl₃ pellet as reference. During in situ studies under dynamic reaction conditions (change of reaction conditions, temperature), faster QEXAFS scans between 22,100 and 22,250 eV were recorded applying the continuous scanning mode (0.18 s/eV).

The raw data were energy calibrated (Ru K-edge energy of RuCl₃: 22.12 keV [38], first inflection point), background corrected and normalized using the WINXAS 3.1 software [38] according to typical procedures described earlier [39,40]. Fourier transformation of EXAFS data was applied to the k^1-weighted functions in the interval $k = 3–13\,\text{Å}^{-1}$. Data fitting was performed in R-space using theoretical backscattering phases and amplitudes calculated with the ab initio multiple scattering code FEFF6.0 [41]. Typical deviations in coordination number are ± 0.5 and for the distance $\pm 0.02\,\text{Å}$.

3. Results and discussion

3.1. Catalyst characterization

The bimetallic RuCoHAp catalyst was characterized by XRD, nitrogen adsorption, ICP-OES, XPS, and thermal analysis [19]. Briefly, in the XRD patterns, only diffraction peaks due to HAp could be seen though the peaks were broader compared to those of HAp, presumably, due to restructuring during incorporation of the metal ions. BET analysis revealed medium surface area ($90\,\text{m}^2\,\text{g}^{-1}$) and a mesoporous structure (average pore diameter: 18 nm) with only a small fraction of microporous area ($7.9\,\text{m}^2\,\text{g}^{-1}$). The $(\text{Ca} + \text{Co} + \text{Ru})/\text{P}$ ratio was 1.51 (ICP-OES), which value is lower than the Ca/P ratio in stoichiometric HAp (1.67 [8]). The catalyst contained 3.5 wt.% Ru and 1.0 wt.% Co and the Cl content was negligible according to ICP-OES and XPS measurements. The binding energy of the Ru $3d_{5/2}$ was observed in RuCoHAp at 281.1 eV, which value is similar to that reported by Wuyts et al. (281.3 eV [18]).
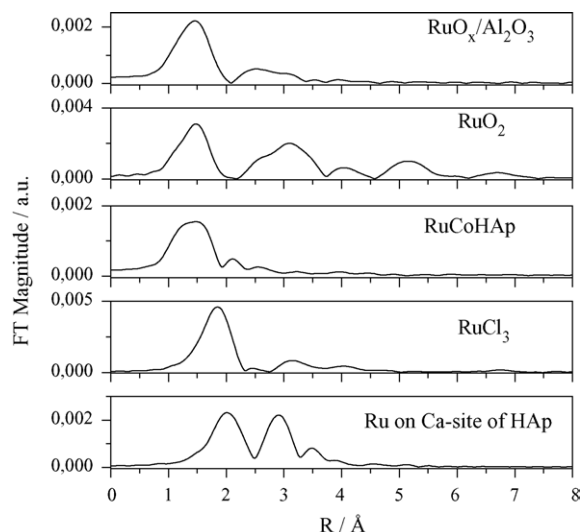

Fig. 1. Fourier-transformed EXAFS data (k^1-weighted $\chi(k)$-function, $3–13\,\text{Å}^{-1}$) of RuO/Al₂O₃, RuO₂, RuCoHAp, and RuCl₃, and the calculated curve of a theoretical RuHAp structure (assuming a simple replacement of a fraction of Ca^{2+} of HAp).

X-ray absorption near-edge structure spectroscopy (XANES) and EXAFS were applied to clarify the nature of the active Ru species. Variations were observed in the XANES spectra of RuCoHAp compared to those of RuO₂ and Ru₂Oₓ/Al₂O₃ (not shown) but no edge shift was detected between Ru^{4+} and Ru^{3+}, which is in accordance with the literature [42]. As Fig. 1 shows, the Fourier-transformed spectrum of RuCoHAp is different from those of the reference samples RuCl₃, RuO₂, and Ru₂Oₓ/Al₂O₃, as well as the model sample (Ru on the Ca site of HAp) calculated by the FEFF code. Obviously, no Ru–Ru contribution above 3 Å is observed, as it is clearly visible in RuO₂, RuOₓ/Al₂O₃, and RuCl₃. Hence, Ru seems to be highly dispersed in hydroxyapatite.

This conclusion is supported also by fitting of the data (Table 1). Scattering events occurring between 1.5 and 2.1 Å can be attributed to oxygen nearest neighbours. Only two oxygen nearest neighbours were fitted. Note, however, that several different species may be present on the surface, including Ru^{3+} species bound to phosphate, calcium, and another Ru^{3+} via oxygen nearest neighbours. The comparison of the EXAFS spectra at the Ru K-edge to the corresponding model spectrum of Ru^{3+} placed on a Ca^{2+} site in HAp (Fig. 1) shows that simple replacement of Ca^{2+} can be excluded, probably because Ru^{3+} is much smaller than Ca^{2+} (Ca^{2+}: 100 pm, Ru^{3+}: 68 pm [43]).

XRD analysis indicated some restructuring during catalyst preparation, when the contact time with RuCl₃ solution was extended from 10 min to 24 h [19]. In contrast, barely any change was found by XANES/EXAFS. Since EXAFS is sensitive to short-range order structures (here, mainly first coordination shell), this observation suggests that already after 10 min contact time an (X-ray amorphous) ruthenium-containing phase was formed.

Table 1

Structural parameters of RuCoHAp and RuO_2 determined by the first shell fitting of EXAFS spectra at the Ru K-edge, compared with structures of various Ru-containing samples taken from the literature

A[a]–Bs[b]	r[c] (Å)	CN[d]	σ^{2}[e] (Å²)	ΔE_0[f] (eV)	Residual[g]
RuCoHAp					
Ru—O	1.88	2.0	0.008	6.1	6.2
Ru—O	1.99	4.3	0.008	−1.14	
Hydrated RuO_2					
Ru[IV]—O	1.91	2.0	0.001	1.24	9.8
Ru[IV]—O	2.01	4.0	0.001	3.83	
$Ru_2P_6O_{18}$[h]					
Ru[III]—O	2.01–2.03	6			
RuHAp[i]					
Ru[III]—O	1.97	4			
Ru[III]—Cl	2.32	1.2			
Cationic RuHAp[j]					
Ru[III]—O(OH₂)	2.10	1			
Ru[III]—O	1.98	4			
Ru/Hydrotalcite[k]					
Ru[IV]—O(OH₂)	1.97	3			
Ru[IV]—O(OH₂)	2.04	2.3			
Ru[IV]—O(OH)	1.82	0.9			
HAp[l]					
Ca—O(OH)	2.37	5.4			
Ca—O	2.56	3			

[a] Absorber atom.
[b] Backscatter atom.
[c] Interatomic distance.
[d] Coordination number.
[e] Debye–Waller factor, set to the same value for both Ru—O shells.
[f] Shift of the energy threshold.
[g] Quality of fit according to Ref. [52].
[h] From the crystallographic data in Ref. [53].
[i] From Ref. [16].
[j] From Ref. [5].
[k] From Ref. [54].
[l] From Ref. [55].

Oxygen contributions at 1.88 and 1.99 Å could be fitted with a higher coordination number for the oxygen backscattering at higher R-values (Table 1). The first shell can be attributed to Ru—OH species, while the other one is probably related to Ru—O—P connectivity (Scheme 2). No Ru—Cl species could be found in the fits. Besides, the chlorine content in the samples was negligible (by ICP-OES and XPS) and also the Fourier-transformed EXAFS spectra depicted in Fig. 1 support the absence of Ru—Cl species. The structure of the highly dispersed Ru species in this study is also
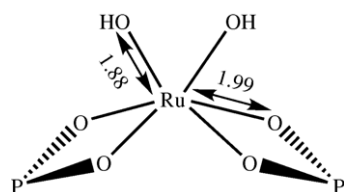
Scheme 2. Proposed structure of the active Ru species in RuCoHAp.

much different from that of the 17 wt.% RuHAp described by Yamaguchi et al. [16], since the oxygen coordination shells were found at much higher R-values. This study supports our former assumption [19] that Ru-OH species are present in RuCoHAp, as depicted in Scheme 2.

Another interesting result is that barely any difference was detectable between the Ru K-EXAFS spectra of RuHAp and RuCoHAp samples. This is an indication that the local structure of Ru is similar in the promoted and unpromoted catalysts. This observation is in line with the suggestion based on XPS analysis that the major role of promotion is the fine tuning of the location of the active Ru species leading to a better accessibility of active sites for the reactant [19].

3.2. In situ EXAFS study

The structure of RuCoHAp during oxidation of benzyl alcohol was investigated in a tiny plug-flow reactor. The thermostated reactor chamber (40 °C) containing the catalyst was first contacted with Ar-saturated toluene, then with an Ar-saturated toluenic solution of benzyl alcohol, and finally, with air-saturated benzyl alcohol solution. The changes observed in the XANES and EXAFS spectra are presented in Fig. 2. The changes were minor upon contacting the catalyst with toluene, but a considerable restructuring was observed after addition of benzyl alcohol in Ar. In contrast to Pd-based catalysts [17,36,37], the ruthenium species were not reduced to Ru^0 by benzyl alcohol under reducing conditions, i.e. in the absence of oxygen. The significant changes in the near-edge structure were maintained, when the feed was changed from Ar-saturated to air-saturated solution of benzyl alcohol. In the EXAFS spectra, the decrease of the shoulder at lower values indicates that the shorter Ru–O bond is exchanged by a longer Ru–O bond, probably due to formation of an alkoxy species.

In the presence of air, 9.0% conversion of benzyl alcohol was achieved after a 70 min stabilization period and no other product beside benzaldehyde was detectable. Approximately, 50% of the oxygen available in the fluid was consumed as calculated from the oxygen solubility in toluene [44]. The reasonably good conversions confirm that the XANES and EXAFS spectra are related to the working catalyst.

3.3. Catalytic studies

The most important application of RuCoHAp catalysts is the oxidation of aromatic alcohols, which reactions are characterized by high rates and better than 99% yields to the corresponding carbonyl compounds [19]. Accordingly, the partial oxidation of benzyl alcohol has been chosen here as a model reaction to study the rate-determining step and the possible reaction mechanism.

Analysis of the reaction rate as a function of conversion revealed a sudden decrease at above ca. 5% conversion. Oxidation of alcohols is accompanied with the formation of equimolar amount of water (Scheme 1). We assume that
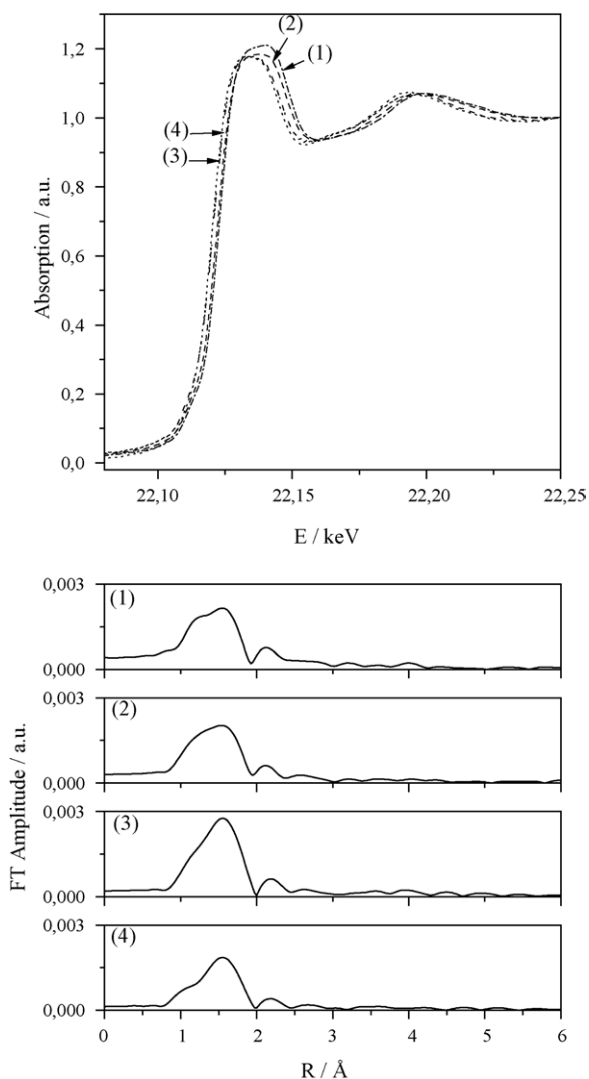
Fig. 2. X-ray absorption near-edge spectra at the Ru K-edge and the corresponding Fourier-transformed EXAFS spectra (k^1-weighted $\chi(k)$-function, 3–13 Å^{-1}) during an in situ experiment at 40 °C with RuCoHAp: (1) before reaction (dash dot); (2) in Ar-saturated toluene (dash); (3) in Ar-saturated toluene at 40 °C with benzyl alcohol (dot); (4) in air saturated toluene at 40 °C with benzyl alcohol (dash dot dot).

water, which dissolves poorly in the apolar reaction medium, accumulates on the polar surface of the catalyst and the hydrated catalyst particles adhere to the reactor wall thereby lowering the efficiency of mass transport. In control experiments, activated molecular sieve was added to the reaction mixture (Fig. 3). When equal amount of catalyst and molecular sieve were used, the initial reaction rate below 5% conversion was not influenced but the subsequent apparent catalyst deactivation could be eliminated. Too high amount of molecular sieve decreased the rate, probably, due to adsorption of the reactant on the molecular sieve and the resulting lower actual reactant concentration in solution. Another, commonly applied solution in synthetic chemistry is to carry out the reaction at reflux temperature, where removal of the co-product water is fast. Under these conditions, however, the actual oxy-
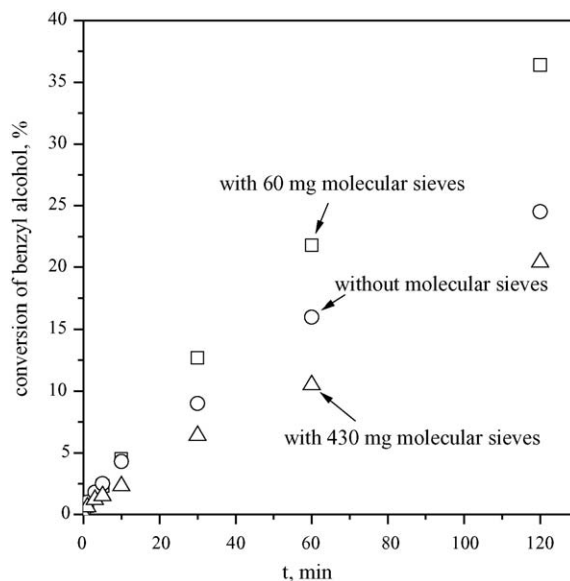

Fig. 3. Effect of molecular sieve on the conversion of benzyl alcohol. *Reaction condition I:* 2 mmol benzyl alcohol; 60 °C; (○) without molecular sieve; (□) with 60 mg molecular sieve; (△) with 430 mg molecular sieve.

gen concentration in solution is poorly defined (equilibrium value is zero) and the stirring efficiency affects the reaction rate.

The dependence of the initial reaction rate (r_0) on the concentration of benzyl alcohol reveals a Michaelis–Menten-type kinetics [45,46]: first-order dependence at low reactant concentration and zero-order dependence at higher concentrations (Fig. 4). First-order correlation indicates that alcohol binding to the catalyst or β-H elimination from the alkoxide is the rate-determining step [47].
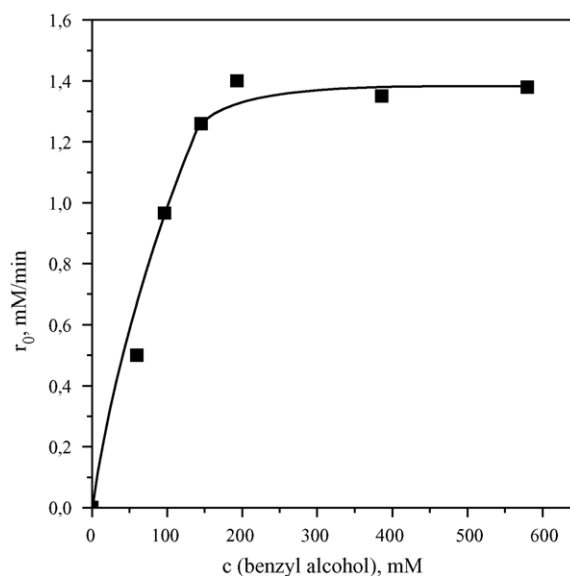

Fig. 4. Influence of benzyl alcohol concentration on the initial rate of its oxidation. *Reaction condition I:* 60 °C.
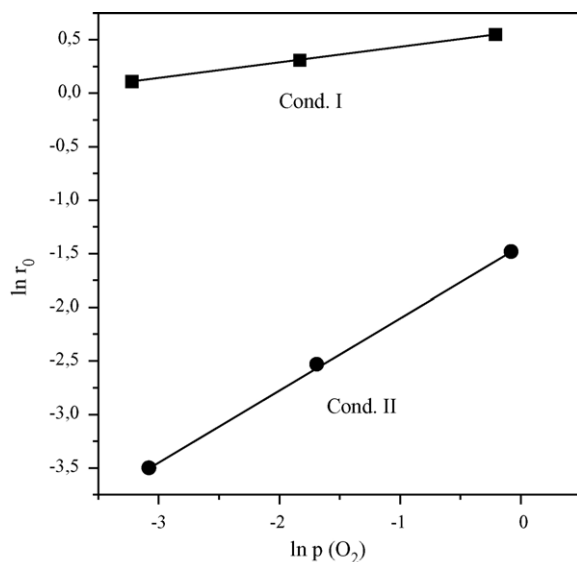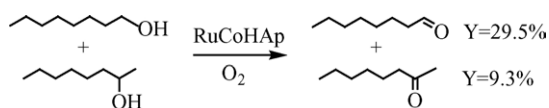
Fig. 5. Influence of oxygen partial pressure on the initial rate of benzyl alcohol oxidation in the kinetic regime (I) and under mass transport limited conditions (II). *Condition I:* (■) 60 mg RuCoHAp; 2 mmol benzyl alcohol; 60 °C. *Condition II:* (●) 52 mg RuCoHAp (0.018 mmol Ru); 0.2 mmol benzyl alcohol; 40 °C.

Fig. 6. Kinetic isotope effect of benzyl alcohol-d_7 in the kinetic regime (I) and under mass transport limited condition (II). *Condition I:* 1 mmol benzyl alcohol (●) or 1 mmol benzyl alcohol-d_7 (○); 60 °C; 60 mg molecular sieve; *condition II:* 1 mmol benzyl alcohol (▲) or 1 mmol benzyl alcohol-d_7 (△); 60 °C; 60 mg molecular sieve.

The initial rate of benzyl alcohol oxidation depended on the O_2 partial pressure (Fig. 5) and this effect was much more pronounced under mass transfer limited conditions, when the actual oxygen concentration on the catalyst surface was low (condition II). This observation indicates that reoxidation of the active Ru species is slow and affects the overall reaction rate, particularly under mass transfer limited conditions. In contrast, the frequently observed zero-order correlation is conform with the high reactivity of the reduced active Ru site (hydride) towards molecular oxygen. Examples include the oxidation of alcohols on Ru/Al_2O_3 [46], RuHAp [16], and HAp-supported Pd [13].

When the reaction was repeated under condition II but in the absence of oxygen (under Ar), transformation of benzyl alcohol ceased after 10 min at 4.7% conversion. This value corresponds to a TON of 0.52. From this experiment, we can conclude that the reaction obeys the Mars–van Krevelen mechanism [48] and in the absence of molecular oxygen the active sites are rapidly reduced and become inactive in the further transformation of benzyl alcohol. The low TON suggests that only about one half of the Ru sites are accessible to the reactant benzyl alcohol.

Competitive oxidation of 1- and 2-octanols uncovered that the primary alcohol was more reactive (Scheme 3). This relation is similar to that observed previously with RuHAp [16].

Scheme 3. Competitive oxidation of 1- and 2-octanol (100 mg RuCoHAp, toluene, 90 °C, 2 h, 100% selectivity to the carbonyl compounds).
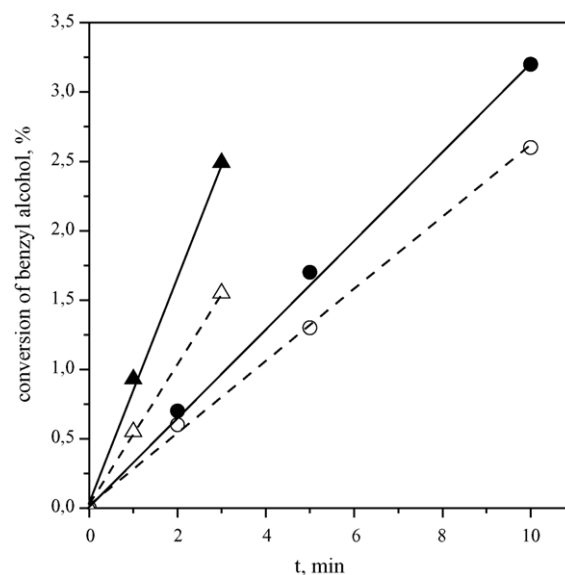
The more than three-fold faster conversion of 1-octanol indicates that Ru–alcoholate is formed in the catalytic cycle as an intermediate [49].

The kinetic isotope effect was also measured in the oxidation of benzyl alcohol and benzyl alcohol-d_7. The oxidation of the two reactants was carried out separately under both conditions to avoid any disturbance by competitive adsorption. The k_H/k_D ratio was calculated from the conversions up to 5%. The k_H/k_D ratio was 1.6 under kinetically controlled condition I and 1.2 under transport limited condition II (Fig. 6). These values are smaller than those found for Ru/Al_2O_3 ($k_H/k_D = 2.4$) [46], $Ru/CeO_2/CoO(OH)$ ($k_H/k_D = 2.5$) [24], and RuHAp ($k_H/k_D = 7.0$) [16], but similar to those obtained with other catalyst systems, such as $Pd(OAc)_2$/pyridine ($k_H/k_D = 1.3$–1.8) [50] and PdHAp ($k_H/k_D = 2.0$). The observed kinetic isotope effect implies that β-hydride elimination from the Ru–alcoholate species may be an important (rate-determining) step in the mechanism of alcohol oxidation. The decrease of the kinetic isotope effect at lower oxygen concentration (Fig. 6) is analogous to the decrease of the kinetic isotope effect with lower TEMPO/Ru ratio in the $RuCl_2(PPh_3)_3$/TEMPO (2,2′,6,6′-tetramethylpiperidinyl-N-oxyl) system ($k_H/k_D = 3.0$ at TEMPO/Ru = 5 and $k_H/k_D = 2.3$ at TEMPO/Ru = 2 at 373 K) [51], where TEMPO plays an important role in the reoxidation of the Ru-hydride species.

The oxidation of p-substituted benzyl alcohols was carried out separately with each alcohol under kinetically controlled condition I. The k_X/k_H values were calculated from the conversions up to 5%. The Hammet plot depicted in Fig. 7 is rather unusual: the decelerating effect of the electron-withdrawing substituents (−NO_2, −Cl) is clearly seen, but the
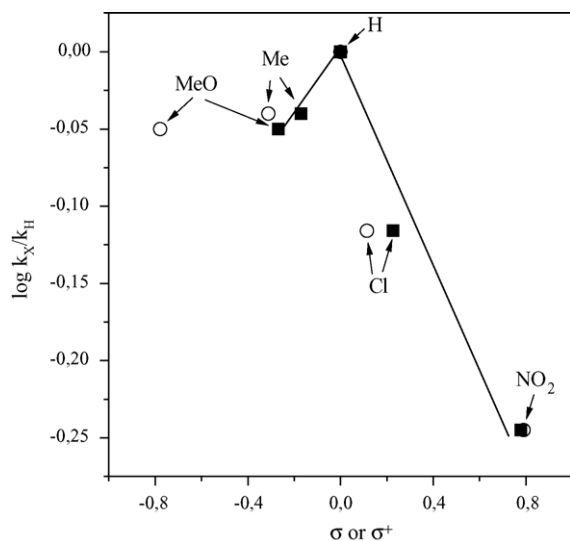
Fig. 7. Hammett plot of *p*-substituted benzyl alcohols. *Reaction condition I:* 1 mmol *p*-X-benzyl alcohol (X = H, Cl, NO$_2$, Me, or MeO), 60 °C; σ (■), σ^+ (○).

Scheme 4. Proposed reaction mechanism for alcohol oxidation over RuCo-HAp.

electron-donating substituents (−MeO, −Me) do not increase the reaction rate. As shown also in Fig. 7, application of the substituent constant σ^+ did not lead to a better fit, which should be the case for the formation of a carbocation transition state [45]. The slope of the Hammett plot ($\rho \approx -0.33$) in the linear part (electron-withdrawing substituents) is smaller than those observed in the oxidation of benzyl alcohol with MnFe$_{1.8}$Cu$_{0.15}$Ru$_{0.05}$O$_4$ ($\rho = -0.9$) [56], RuHAp ($\rho = -0.43$) [16], RuCl$_2$(PPh$_3$)$_3$ ($\rho = -0.44$ by TEMPO/Ru = 2:1 and −0.58 by TEMPO/Ru = 6:1) [51] and Ru/Al$_2$O$_3$ ($\rho = -0.46$) [46]. According to the conventional interpretation, negative ρ values indicate migration of H with partial hydride character, though other explanations involving the stability of the carbocation intermediate or the resulting electron-rich ketone complex are also feasible [47].

3.4. Mechanistic considerations

The probable reaction route, based on the catalytic and XAS measurements and literature data, is shown in Scheme 4. Alcohol oxidation through the hydridometal pathway [23] generally involves the formation of a Ru–alcoholate species (step 1), which undergoes β-hydride elimination to produce the carbonyl compound and a hydrido-ruthenium species (step 2). The hydrido-ruthenium species is then reoxidized by molecular oxygen to close the catalytic cycle (step 3).

The higher reactivity of primary alcohols relative to that of secondary alcohols (Scheme 3) and the dependence of the reaction rate on alcohol concentration (Fig. 4) and support steps 1 and 2 in Scheme 4. The importance of reoxidation of the Ru-hydrido species, and thus, regeneration of the active species (step 3 in Scheme 4) is confirmed by three important observations. The actual oxygen concentration, controlled by the rate of oxygen supply to the catalyst surface relative to
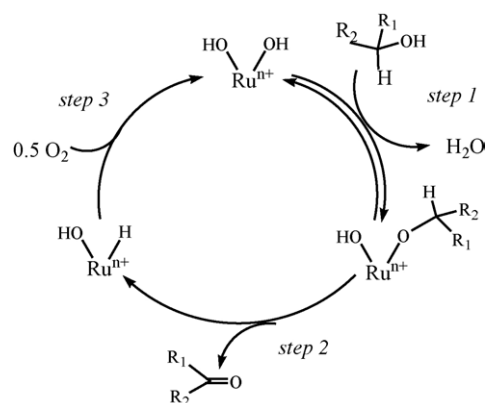
the rate of alcohol dehydrogenation, had a strong influence on the overall reaction rate, particularly under oxygen starvation conditions (Fig. 5). In the absence of molecular oxygen the oxidation of benzyl alcohol stopped at 4.7% conversion (TON = 0.52), indicating that the reduced Ru sites are inactive. Besides, the in situ EXAFS analysis (Fig. 2) revealed that during oxidation of benzyl alcohol the Ru active sites were – at least partly – in a reduced state that may correspond to the Ru-hydrido species.

As concerns the rate-determining step, interpretation of the results is not straightforward. We attribute the apparent contradiction to the comparable rates of β-hydride elimination (step 2) and reoxidation of the Ru-hydrido species (step 3 in Scheme 4). Depending on the reaction conditions, either step 2 or step 3 becomes rate limiting, that is dehydrogenation plays a more important role at high O$_2$ concentration and reoxidation at low O$_2$ concentration. This interpretation is supported by the influence of oxygen transport limitation on the primary kinetic isotope effect and the close analogy to the kinetic isotope effect measured with the RuCl$_2$(PPh$_3$)$_3$/TEMPO system at various TEMPO/Ru ratios [51]. The dependence of the initial reaction rate on the oxygen pressure and the rate of mass transport (Fig. 5) provides further support to this assumption.

A shift in the rate-determining step can explain the unusual Hammett plot (Fig. 7). In the oxidation of *para*-substituted benzyl alcohols, electron-donating substituents in *p*-position should accelerate the reaction by stabilizing the carbocation intermediate, and electron-withdrawing substituents should decelerate it, if the dehydrogenation is the rate-determining step. The missing accelerating effect of electron-donating substituents may indicate that the dehydrogenation becomes so fast that it is not any more rate limiting. Besides, the reaction rate is presumably distorted also by the different adsorption strength of the *p*-substituted benzyl alcohols leading to different surface concentrations; this effect is absent in homogeneous catalysis, where the method is mainly used to study reaction mechanisms.

In the in situ EXAFS experiments, two important changes were observed after addition of benzyl alcohol under Ar to the reaction mixture. The change of the near-edge structure, the small shift toward lower threshold energy, is attributed to the reduction of ruthenium in the catalyst. No Ru metal is observed even in the absence of oxygen that supports the mechanism involving ionized Ru species (Scheme 4). Furthermore, the decrease of the shoulder at lower values, the short Ru−O(OH) bond in the Fourier-transformed EXAFS spectra, suggests the formation of Ru–alcoholate species by ligand exchange between the OH group and the alcoholate group (Scheme 4, step 1). After admission of oxygen, reoxidation of the catalyst (step 3) and a shift of the edge back toward higher threshold energy would be expected. We did not observe these changes, which indicate that the reoxidation step is slow compared to the other steps. Under the oxygen transport limited conditions of the in situ EXAFS experiment reoxidation of the Ru-species is the rate-determining step.

4. Conclusions

The aim of the present study was to clarify some points in the mechanism of alcohol oxidation on Ru-containing hydroxyapatite, RuHAp. A highly active Co-promoted catalyst, RuCoHAp was selected for the catalytic and (in situ) XANES/EXAFS investigations. The spectroscopic method confirmed the presence of highly dispersed, ionic Ru^{n+} species with the most probable structure of $Ru^{n+}(OH)_2$. A detailed kinetic analysis of benzyl alcohols revealed that both β-hydride elimination from the ruthenium-alcoholate intermediate and reoxidation of the ruthenium-hydrido species may be the rate limiting step in the reaction mechanism. Catalyst reoxidation becomes important only when dehydrogenation of the alcohol reactant is fast, relative to the rate of oxygen supply to the active sites located in the catalyst pores. An obvious conclusion is that in the oxidation of aliphatic and cycloaliphatic alcohols, which are less reactive than the aromatic alcohols, reoxidation of the ruthenium sites should not limit the overall reaction rate.

References

[1] M. Besson, P. Gallezot, Catal. Today 57 (2000) 127.
[2] J.H.J. Kluytmans, A.P. Markusse, B.F.M. Kuster, G.B. Marin, J.C. Schouten, Catal. Today 57 (2000) 143.
[3] B.Z. Zhan, A. Thompson, Tetrahedron 60 (2004) 2917.
[4] T. Mallat, A. Baiker, Chem. Rev 104 (2004) 3037.
[5] K. Kaneda, K. Mori, T. Hara, T. Mizugaki, K. Ebitani, Catal. Surv. Asia 8 (2004) 231.
[6] C.L. Kibby, S.S. Lande, W.K. Hall, J. Am. Chem. Soc. 94 (1972) 214.
[7] C.L. Kibby, W.K. Hall, J. Catal. 29 (1973) 144.
[8] S. Sugiyama, T. Minami, H. Hayashi, M. Tanaka, N. Shigemoto, J.B. Moffat, J. Chem. Soc. Faraday Trans. 92 (1996) 293.
[9] S. Sugiyama, T. Shono, E. Nitta, H. Hayashi, Appl. Catal. A 211 (2001) 123.
[10] S. Sebti, R. Tahir, R. Nazih, A. Saber, S. Boulaajaj, Appl. Catal. A 228 (2002) 155.
[11] S. Sebti, R. Tahir, R. Nazih, S. Boulaajaj, Appl. Catal. A 218 (2001) 25.
[12] M. Zahouily, Y. Abrouki, B. Bahlaouan, A. Rayadh, S. Sebti, Catal. Commun. 4 (2003) 521.
[13] K. Mori, T. Hara, T. Mizugaki, K. Ebitani, K. Kaneda, J. Am. Chem. Soc. 126 (2004) 10657.
[14] A. Venugopal, M.S. Scurrell, Appl. Catal. A 245 (2003) 137.
[15] C.M. Ho, W.Y. Yu, C.M. Che, Angew. Chem. Int. Ed. 43 (2004) 3303.
[16] K. Yamaguchi, K. Mori, T. Mizugaki, K. Ebitani, K. Kaneda, J. Am. Chem. Soc. 122 (2000) 7144.
[17] K. Mori, K. Yamaguchi, T. Hara, T. Mizugaki, K. Ebitani, K. Kaneda, J. Am. Chem. Soc. 124 (2002) 11572.
[18] S. Wuyts, D.E. De Vos, F. Verpoort, D. Depla, R. De Gryse, P.A. Jacobs, J. Catal. 219 (2003) 417.
[19] Z. Opre, J.D. Grunwaldt, M. Maciejewski, D. Ferri, T. Mallat, A. Baiker, J. Catal. 230 (2005) 406.
[20] K. Elkabouss, M. Kacimi, M. Ziyad, S. Ammar, F. Bozon-Verduraz, J. Catal. 226 (2004) 16.
[21] M. Wakamura, K. Kandori, T. Ishikawa, Colloid Surf. A 164 (2000) 297.
[22] M. Wakamura, K. Kandori, T. Ishikawa, Colloid Surf. A 142 (1998) 107.
[23] I.W.C.E. Arends, T. Kodama, R.A. Sheldon, Top. Organometal. Chem. 11 (2004) 277.
[24] K. Ebitani, H.B. Ji, T. Mizugaki, K. Kaneda, J. Mol. Catal. A 212 (2004) 161.
[25] B.Z. Zhan, M.A. White, T.K. Sham, J.A. Pincock, R.J. Doucet, K.V.R. Rao, K.N. Robertson, T.S. Cameron, J. Am. Chem. Soc. 125 (2003) 2195.
[26] T.L. Stuchinskaya, M. Musawir, E.F. Kozhevnikova, I.V. Kozhevnikov, J. Catal. 231 (2005) 41.
[27] S.V. Dorozhkin, Prog. Cryst. Growth Charact. Mater. 44 (2002) 45.
[28] E. Valsami-Jones, K.V. Ragnarsdottir, A. Putnis, D. Bosbach, A.J. Kemp, G. Cressey, Chem. Geol. 151 (1998) 215.
[29] B.S. Clausen, H. Topsoe, R. Frahm, Advances in Catalysis, vol. 42, 1998, p. 315.
[30] J.M. Thomas, G. Sankar, J. Synchrotron. Radiat. 8 (2001) 55.
[31] J.D. Grunwaldt, M. Caravati, S. Hannemann, A. Baiker, Phys. Chem. Chem. Phys. 6 (2004) 3037.
[32] M. Fernandez-Garcia, Catal. Rev. Sci. Eng. 44 (2002) 59.
[33] J.D. Grunwaldt, B.S. Clausen, Top. Catal. 18 (2002) 37.
[34] A.P. Markusse, B.F.M. Kuster, D.C. Koningsberger, G.B. Marin, Catal. Lett. 55 (1998) 141.
[35] A. Edelmann, W. Schiesser, H. Vinek, A. Jentys, Catal. Lett. 69 (2000) 11.
[36] J.D. Grunwaldt, C. Keresszegi, T. Mallat, A. Baiker, J. Catal. 213 (2003) 291.
[37] C. Keresszegi, J.D. Grunwaldt, T. Mallat, A. Baiker, J. Catal. 222 (2004) 268.
[38] K. Okamoto, T. Takahashi, K. Kohdate, H. Kondoh, T. Yokoyama, T. Ohta, J. Synchrotron. Radiat. 8 (2001) 689.
[39] B.K. Theo, EXAFS: Basic Principles and Data Analysis, Springer, Berlin, 1986.
[40] D.C. Koningsberger, R. Prins, X-ray Absorption: Principles, Applications, Techniques of EXAFS, SEXAFS, and XANES, Wiley, New York, 1988.
[41] S.I. Zabinsky, J.J. Rehr, A. Ankudinov, R.C. Albers, M.J. Eller, Phys. Rev. B 52 (1995) 2995.
[42] D.A. McKeown, P.L. Hagans, L.P.L. Carette, A.E. Russell, K.E. Swider, D.R. Rolison, J. Phys. Chem. B 103 (1999) 4825.
[43] R.D. Shannon, Acta Crystallogr. Sect. A Found. Crystallogr. 32 (1976) 751.
[44] K. Fischer, M. Wilken, J. Chem. Thermodyn. 33 (2001) 1285.

[45] K.A. Connors, Chemical Kinetics: The Study of Reaction Rates in Solution, VCH, New York, 1990.

[46] K. Yamaguchi, N. Mizuno, Chem. Eur. J. 9 (2003) 4353.

[47] J.A. Mueller, D.R. Jensen, M.S. Sigman, J. Am. Chem. Soc. 124 (2002) 8202.

[48] C. Doornkamp, V. Ponec, J. Mol. Catal. A Chem. 162 (2000) 19.

[49] G.J. ten Brink, I. Arends, R.A. Sheldon, Adv. Synth. Catal. 344 (2002) 355.

[50] B.A. Steinhoff, S.S. Stahl, Org. Lett. 4 (2002) 4179.

[51] A. Dijksman, A. Marino-Gonzalez, A.M.I. Payeras, I. Arends, R.A. Sheldon, J. Am. Chem. Soc. 123 (2001) 6826.

[52] T. Ressler, J. Synchrotron. Radiat. 5 (1998) 118.

[53] H. Fukuoka, H. Imoto, T. Saito, J. Solid State Chem. 119 (1995) 107.

[54] K. Motokura, D. Nishimura, K. Mori, T. Mizugaki, K. Ebitani, K. Kaneda, J. Am. Chem. Soc. 126 (2004) 5662.

[55] J.E. Harries, D.W.L. Hukins, S.S. Hasnain, J. Phys. C Solid State Phys. 19 (1986) 6859.

[56] H.B. Ji, L.F. Wang, Chin. J. Chem. 20 (2002) 944.